

Article

A Resonant Hybrid DC Circuit Breaker for Multi-Terminal HVDC Systems

Ryo Miyara ^{1,*}, Akito Nakadomari ¹ , Hidehito Matayoshi ², Hiroshi Takahashi ³, Ashraf M. Hemeida ⁴  and Tomonobu Senju ^{1,*} 

¹ Faculty of Engineering, University of the Ryukyus, 1 Senbaru, Nishihara-cho, Nakagami, Okinawa 903-0213, Japan; akito.nakadomari@gmail.com

² Osaka Institute of Technology, Osaka 530-8568, Japan; hidehito.matayoshi@oit.ac.jp

³ Fuji Electric Co., Ltd., Tokyo 141-0032, Japan; takahashi-hiroshi@fujielectric.com

⁴ Department of Electrical Engineering, Faculty of Energy Engineering, Aswan University, Aswan 51528, Egypt; ashraf@aswu.edu.eg

* Correspondence: e175317h@gmail.com (R.M.); b985542@tec.u-ryukyu.ac.jp (T.S.); Tel.: +81-98-895-8589 (T.S.)

Received: 26 July 2020; Accepted: 18 September 2020; Published: 20 September 2020



Abstract: High-voltage direct current (DC) transmission systems and multi-terminal direct current transmission systems are attracting attention for expanding the grid to promote introduction of renewable energy. Fault clearing in DC systems is difficult because there is no zero point of current. Hybrid circuit breakers are suitable for fault clearing in DC systems. Conventional hybrid circuit breakers have a hard-switching path that damages the switch. Hard switching damages the device and produces emissions due to harmonic noise. A novel resonant hybrid DC circuit breaker is proposed in this paper. The proposed circuit breaker reduces the damage to the switching device using soft switching due to the current zero point. The proposed circuit breaker is compared with conventional hybrid circuit breakers using numerical simulations. Interruption times and switching types of circuit breakers were compared. The simulation results of the fault clearing characteristics of the proposed breakers show that the proposed breakers have sufficient performance and are capable of stable reconnections in multi-terminal direct current transmission systems.

Keywords: HVDC; MTDC; hybrid DC circuit breaker; fault clearing; ZCS; HB-MMC

1. Introduction

The introduction of renewable energy sources (RESs), such as wind generators and photovoltaic generators, has been advancing in recent years [1–3]. However, power quality is reduced by the unstable output of RESs [4]. This problem is solved by a smoothing effect through the power system's expansion. The generation fluctuations of many RESs cancel each other out to yield the total system generation in a large area that fluctuates less [5,6]. Therefore, power system expansion is required. High-voltage direct current (HVDC) transmission and multi-terminal direct current (MTDC) transmission have attracted attention for system expansions [7–10]. Direct current (DC) systems are more efficient than alternating current (AC) systems in long-distance transmission [11]. Furthermore, there are no problems with inductance, capacitance, and phase displacement, which are common in AC transmission.

Modular multilevel converter (MMCs) attracted attention as grid-connected converters [12,13]. An MMC is composed of a number of cascaded cells and outputs voltages that are close to sine waveforms through multi-level conversion [14,15]. MMC cells are classified into half-bridge (HB) cells and full-bridge (FB) cells [16]. FB cells have four semiconductor switches per cell. HB cells have two semiconductor switches per cell. The advantage of HB cells is that HB cells cost less than FB cells and have lower steady-state conduction losses because of the smaller number of switching devices.

The advantage of FB cells is that they have a fault interruption capability [17]. However, because it blocks all converters connected to the grid, it is not possible to identify the point of failure. In addition, this clearing method requires a long preparation time for restoration [17]. HB cells do not have a fault interruption capability. A DC circuit breaker solves this problem.

DC fault interruption is difficult because there are no current zero points [18–21]. DC circuit breakers are the most reliable in fault interruption in DC systems [22]. There are three main types of DC circuit breakers: mechanical circuit breakers, semiconductor circuit breakers, and hybrid circuit breakers [23]. The response of mechanical circuit breakers is slow. Semiconductor circuit breakers have a steady-state loss problem. In 2012, a hybrid circuit breaker with high speed and low steady-state loss was developed by Asea Brown Boveri (ABB) Ltd [24]. A hybrid circuit breaker is shown in Figure 1. A hybrid circuit breaker has a main path consisting of an ultrafast disconnecter (UFD) and a load commutation switch (LCS), as well as a breaker path consisting of many semiconductor switches and a metal oxide varistor (MOV). The operation of a hybrid circuit breaker is shown in Figure 2 [25]. The main path carries the current during normal operation (a). When a fault is detected, the LCS is switched off immediately; hence, the fault current starts to be commutated to the breaker path (b). The UFD begins to open after the transition. The fault current flowing through the semiconductor switches in the breaker path increases until the UFD opens. When the UFD is fully open, the breaker path's semiconductor switches are turned off, and the current is commutated to the MOV (c). The MOV reduces the current and eliminates the fault. In the process of (b)–(c), the semiconductor switch in the breaker path rapidly turns off the high current and uses hard switching. Hard switching can exceed the reverse bias safety operation area (RBSOA) and cause significant damage to semiconductor devices [26]. In addition, hard switching causes electromagnetic interference (EMI) due to high-frequency noise [27].

A novel resonant hybrid DC circuit breaker is proposed in this paper. The proposed circuit breaker creates a current zero point. Zero-current switching (ZCS) avoids the negative effects of hard switching. A fault in an MTDC system was simulated to verify the practicality of the proposed circuit breaker. The proposed circuit breaker's interruption time is sufficiently short and provides stable power transmission during faults. The effectiveness of the proposed method was verified by MATLAB/Simulink simulations.

The remaining sections of the paper discuss the following: Section 2 describes a fault in the HB–MMC system. Section 3 explains the configuration of the MTDC system and the proposed hybrid circuit breaker. Section 4 discusses the principle of operation of the proposed circuit breaker. Section 5 presents the simulation results. Finally, Section 6 presents the inferences and conclusions concerning the proposed idea.

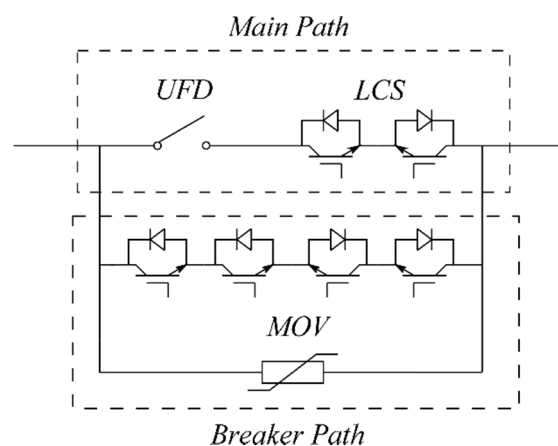


Figure 1. Hybrid direct current (DC) breaker proposed by ABB.

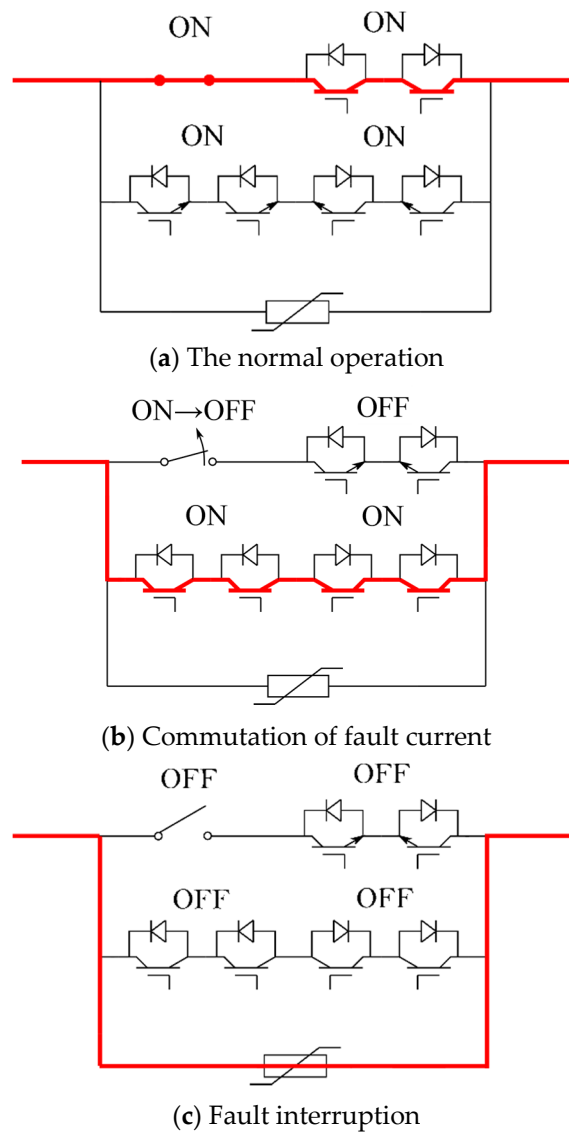


Figure 2. Operation principle of ABB’s hybrid DC breaker. (a) The normal operation; (b) Commutation of fault current; (c) Fault interruption.

2. Analysis of an HB–MMC System Fault

An equivalent circuit of an HB–MMC during a fault is shown in Figure 3 [28]. The MMC operates as a converter during the fault. The equivalent circuit at fault consists of a circuit of resistance R , inductance L and capacitor C . The conditions for the current to create a zero point are represented by Equation (1).

$$\frac{R}{2} < \sqrt{\frac{L}{C}} \tag{1}$$

where $\alpha = \frac{R}{2L}, \beta = \frac{1}{2L} \sqrt{\frac{4L}{C} - R^2}$.

Let the initial current be i_0 ; the fault current $i(t)$ is represented by Equation (2) [2].

$$i(t) = i_0 + \frac{E}{\beta L} e^{-\alpha t} \sin \beta t \tag{2}$$

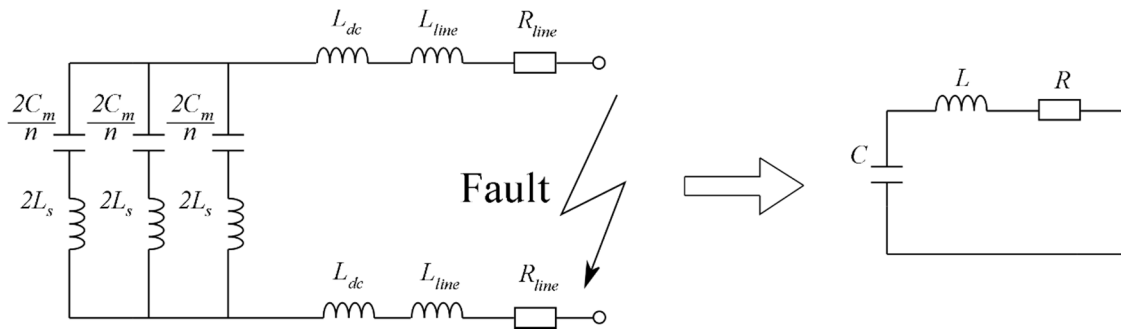


Figure 3. Equivalent circuit during the fault of HB-MMC.

3. Configuration of the MTDC System and Circuit Breaker

3.1. Configuration of the MTDC System

In this paper, a modular multi-level converter is adopted as the AC/DC converter for the MTDC system. The configuration of the MMC is shown in Figure 4 [17]. The number of submodule stages is four. The configuration of the HB cell is shown in Figure 5 [17]. The HB-MMC-MTDC system assumed in this paper is shown in Figure 6 [29]. Power flow control between the four regions of the MTDC system is achieved by the MMC. The MTDC system’s parameters are listed in Table 1. The transmission line model is shown in Figure 7 [30].

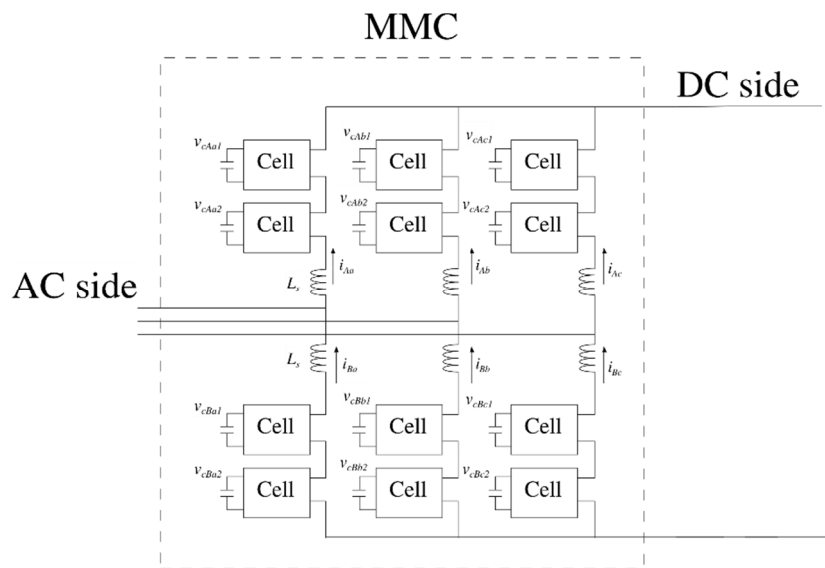


Figure 4. Modular multi-level converter (MMC).

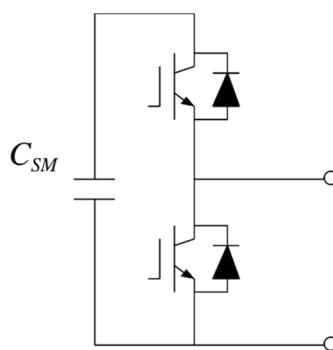


Figure 5. Half-bridge (HB) cells.

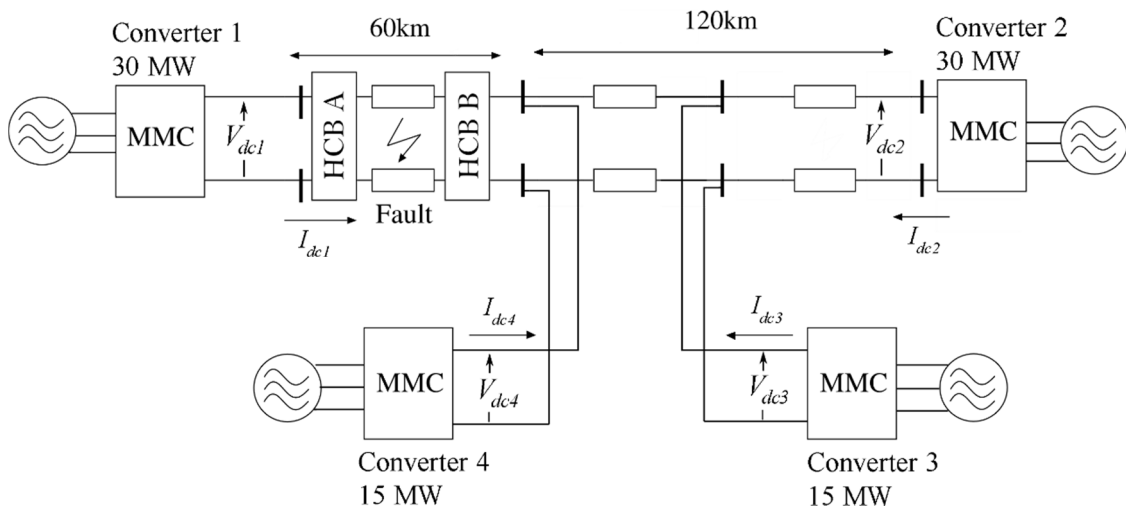


Figure 6. HB-MMC-MTDC system.

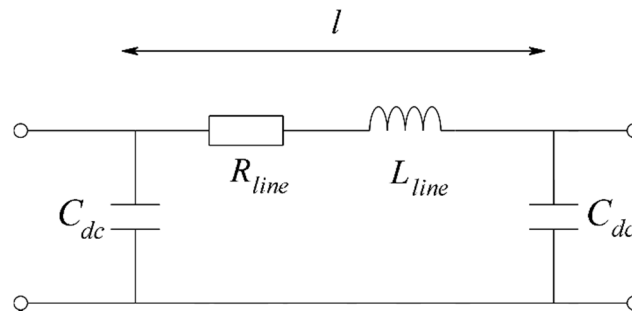


Figure 7. Transmission line model.

Table 1. Parameters of the HB-MMC-MTDC system.

Parameters	Symbol	Value
DC link voltage	$V_{dc1}, V_{dc2}, V_{dc3}, V_{dc4}$	150 kV
Transmission distance	l	120 km
Resistor of transmission line	R_{line}	1.39 mΩ/km
Inductance of transmission line	L_{line}	0.159 mH/km
DC capacitor	C_{dc}	300 μF
DC inductance	L_{dc}	100 mH
Suppression inductance	L_s	100 mH
Cell capacitor	C_{SM}	300 μF

3.2. Configuration of Circuit Breaker

The proposed resonant hybrid DC circuit breaker is shown in Figure 8. The hybrid circuit breaker consists of a mechanical switch, a semiconductor switch, a resonant circuit, and a demagnetization circuit. The mechanical switch conducts during normal operation. The semiconductor switch operates the resonant circuit to generate a current zero point on the transmission line at the time of the fault. ZCS avoids the negative effects of hard switching. Moreover, the residual inductance is low and the energy to demagnetize is low. The proposed circuit breaker is installed on the DC side of each converter, as shown in Figure 6. The circuit breaker limits the fault section and reduces the impact on other systems. In addition, the circuit breakers are connected in close proximity between the converters, and the AC system is largely unaffected by the DC faults. The parameters of the proposed breaker are shown in Table 2.

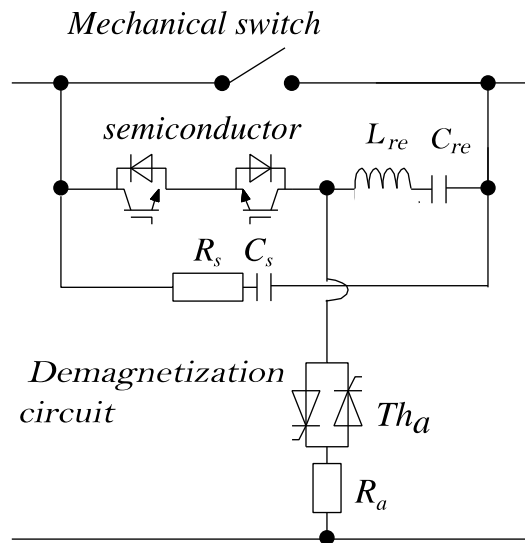


Figure 8. Resonant DC circuit breaker.

Table 2. Parameters of the hybrid circuit breaker.

Parameters	Symbol	Value
Demagnetization resistor	R_a	10 Ω
Resonant capacitor	C_{re}	1 μF
Resonant inductance	L_{re}	1 mH
Snubber resistor	R_s	500 Ω
Snubber capacitor	C_s	0.08 μF

3.3. Parameter Design

The MMC during the failure is represented in Figure 3. Considering $n = 4$, R , L , and C are represented by Equations (3)–(5).

$$R = 2R_{line} = 2 \times R_l \times \frac{l}{2} = 2 \times 1.39 \times 10^{-3} \times 60 = 0.1668[\Omega] \quad (3)$$

$$L = \frac{2L_s}{3} + 2L_{line} + 2L_{dc} + L_{re} = \frac{2 \times 100 \times 10^{-3}}{3} + 2 \times 0.159 \times 10^{-3} \times 60 + 2 \times 100 \times 10^{-3} + L_{re} = 285.7 + L_{re}[\text{mH}] \quad (4)$$

$$C = \frac{\frac{3}{2}C_m C_{re}}{\frac{3}{2}C_m + C_{re}} = \frac{\frac{3}{2} \times 300 \times 10^{-6}}{\frac{3}{2} \times 300 \times 10^{-6} + C_{re}} C_{re} = \frac{450}{450 + C_{re}} C_{re}[\mu\text{F}] \quad (5)$$

The condition for having a current zero point is given by Equation (2). Assuming the inductor to be 1 mH, the condition of the resonant capacitor is represented by Equation (6).

$$C_{re} < 2.16 \times 10^{-5}[\text{F}] \quad (6)$$

Considering the calculation error, $C_{re} = 1[\mu\text{F}]$.

4. Operation Principle of the Circuit Breaker

The operation of the proposed breaker is shown in Figure 9. In the case of a fault, the current is increased towards the fault point (a). The semiconductor switch and the resonant circuit are turned on after detecting a drop in DC transmission voltage or a rise in DC current due to the fault (b). The impedance at the semiconductor branch approaches zero due to the resonance phenomenon. Therefore, the rectification of the semiconductor switch creates a current zero point at the mechanical

switch. The mechanical switch turns off at the current zero point (c). After the mechanical switch is turned off, the semiconductor switch turns off at the current zero point. After the current interruption, the thyristor *Tha* is turned on and the residual inductance is demagnetized (d).

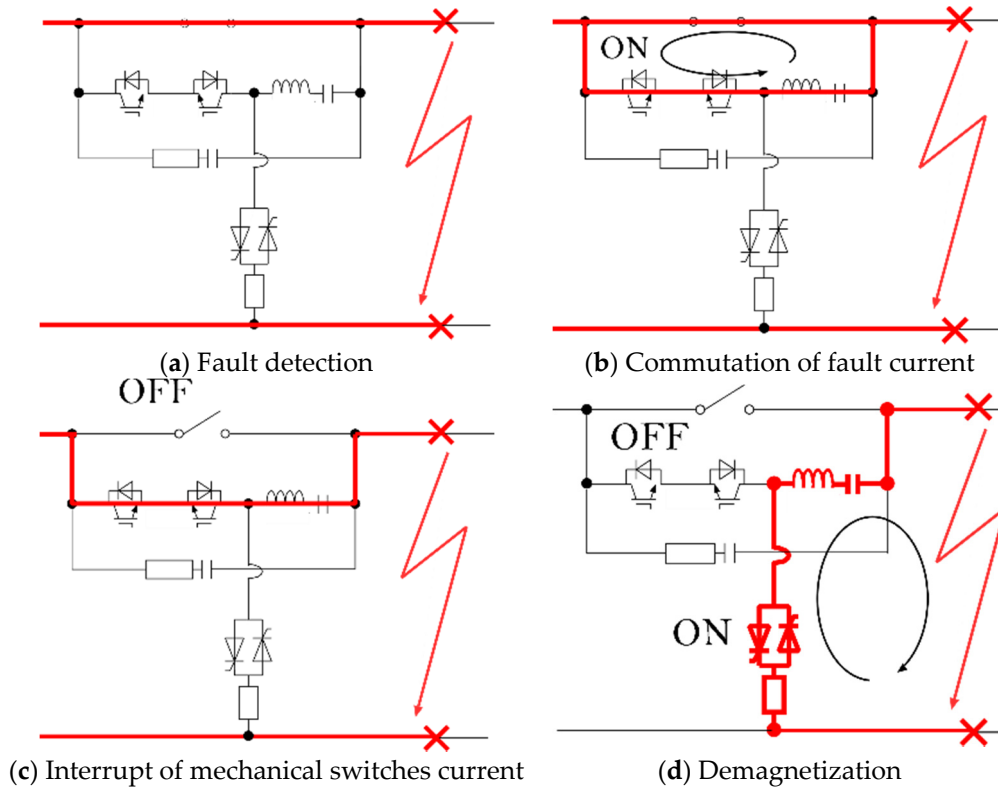


Figure 9. Principle of circuit breaker operation. (a) Fault detection; (b) Commutation of fault current; (c) Interrupt of mechanical switches current; (d) Demagnetization.

5. Simulations

5.1. Simulation Conditions

In this paper, the fault clearing characteristics and a system restart are simulated in the case of a short-circuit fault. The system was simulated in MATLAB/Simulink and was modeled as follows.

- The AC system assumed to have a 230 kV, three-phase AC power supply.
- The fault detection method is shown in Figure 10. A fault is determined when the voltage is less than 100 kV and the current exceeds 300 A.

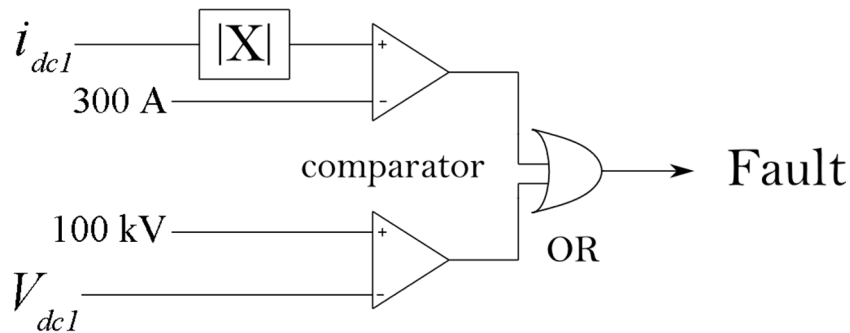


Figure 10. Fault detection method.

The DC fault current interruption characteristics of the ABB's hybrid circuit breaker are simulated for comparison with the proposed circuit breaker. The ABB's hybrid circuit breaker is shown in Figure 1. Assuming that the time to open the UFD takes 1.5 ms, hard switching of the circuit breaker is observed. The circuit breaker's interruption time should be within 5 ms [24]. If the proposed circuit breaker has an interrupting capability within 5 ms and achieves ZCS, the effectiveness of the proposed method is demonstrated.

The proposed circuit breaker simulated the fault interruption of the MTDC system. The sequence of the fault interruption simulation is as follows. A short-circuit failure occurs in the MTDC system at $t = 3$. After the fault clearing, the circuit breaker is re-closed and power transmission resumes from $t = 3.3$ s. The utility of the proposed circuit breaker is demonstrated when the effective power of each system is stable and restored.

5.2. Simulation Results of the ABB's Breaker

Figure 11 shows the mechanical switch current and Figure 12 shows the semiconductor switch current. When a fault is detected, the LCS is turned off and the current in the mechanical switch generates a current zero point. The current in the semiconductor switch is rectified and flows into the MOV when the UFD opens. The MOV current is shown in Figure 13. Current is reduced and fault clearing is achieved. The current interruption time is 1.5 ms. In Figure 12, the semiconductor switch is turned off rapidly from 2 kA. In these simulation results, the hard switching of conventional hybrid circuit breakers was observed.

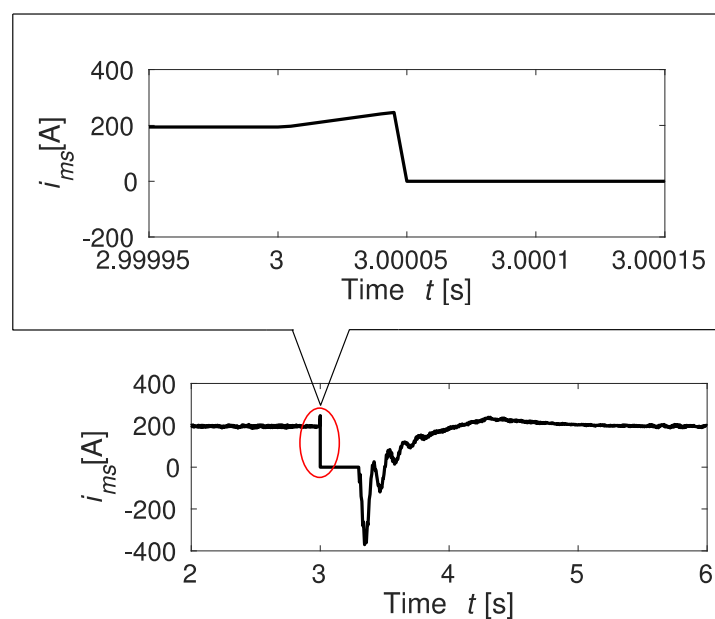


Figure 11. Current of the mechanical switch (ABB).

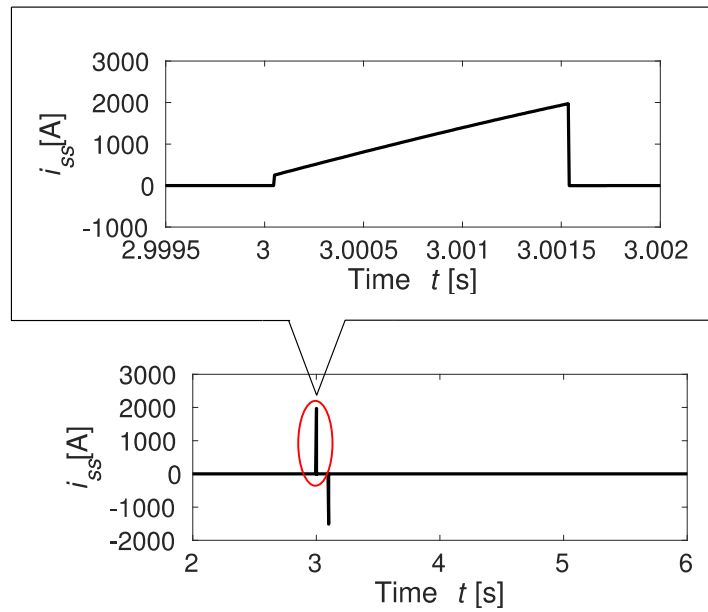


Figure 12. Current of the semiconductor switch (ABB).

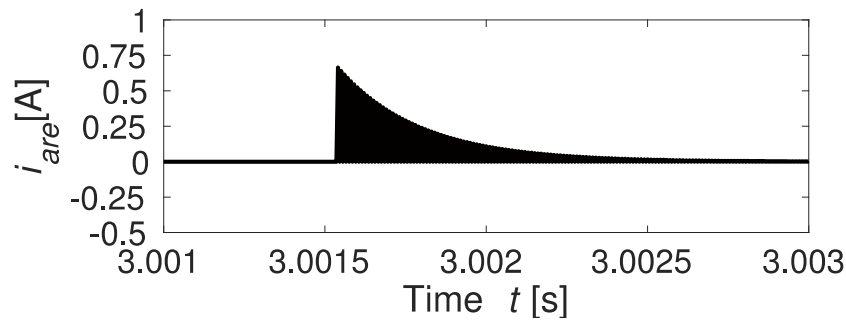


Figure 13. Current of the surge arrester (ABB).

5.3. Simulation Results of the Proposed Breaker

The current of a mechanical switch is shown in Figure 14 and the current of a semiconductor switch is shown in Figure 15. The mechanical switch is found to pass through the zero point during rectification to complete the interruption. The semiconductor switch current is interrupted at the current zero point. The current interruption time is between 1 and 1.1 ms. ZCS can be observed in Figure 15.

The transmission line current is shown in Figure 16 and the transmission line voltage is shown in Figure 17. In the case of the fault, the transmission of power to other systems is stable and voltage fluctuations are controlled. The submodule capacitor voltage of the MMC at the point of fault is shown Figure 18. The submodule capacitor voltage outside the point of fault is shown in Figure 19. The voltage fluctuation is small and stable, and protection of the MMC is achieved. The active power of each converter is shown in Figure 20. The fault point's active power P_1 has zero power, and the other systems are making up for the lack of power. At $t = 3.3$ s, the system is restarted. When reconnected, the time required to recover the current is 1 s. In these simulation results, the proposed circuit breaker achieves soft-switching fault interruption. In addition, the reconnections are smooth. Therefore, the practicality of the proposed circuit breaker has been demonstrated.

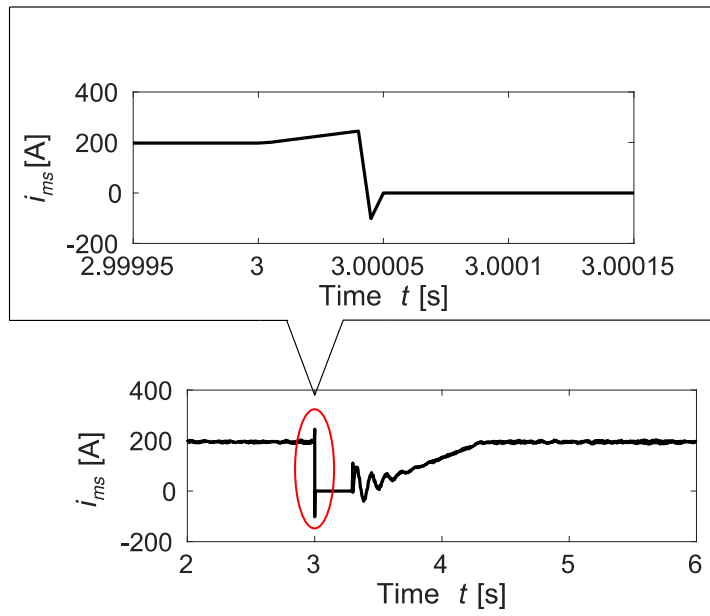


Figure 14. Current of the mechanical switch.

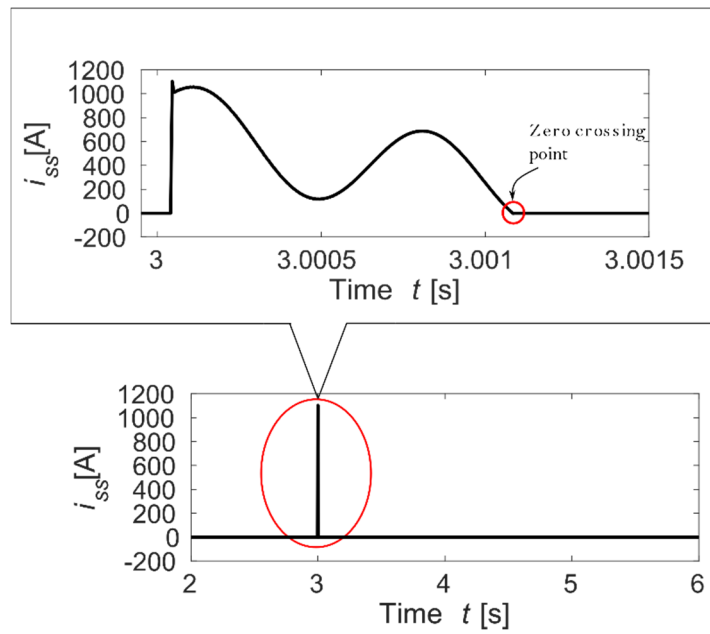


Figure 15. Current of the semiconductor switch.

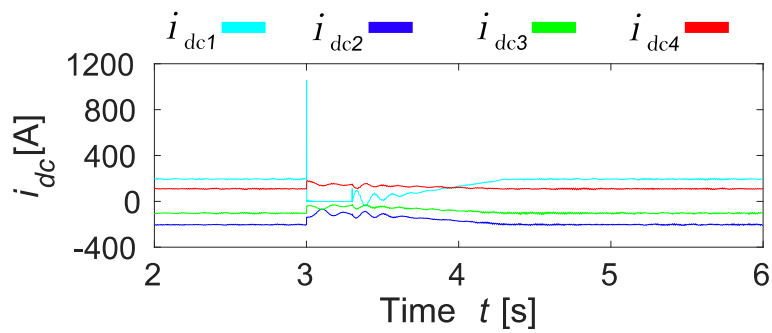


Figure 16. Current of the transmission line.

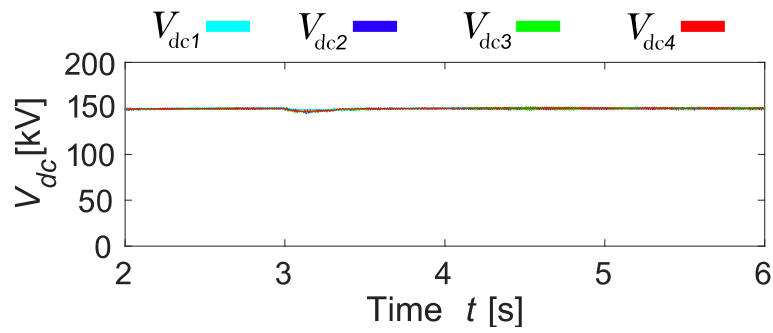


Figure 17. Transmission line voltage.

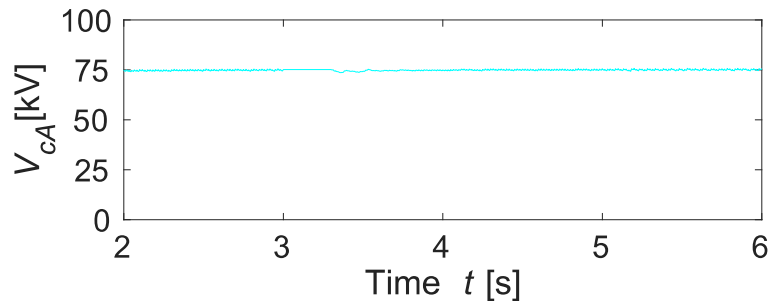


Figure 18. The voltage of the submodule capacitor at the fault points.

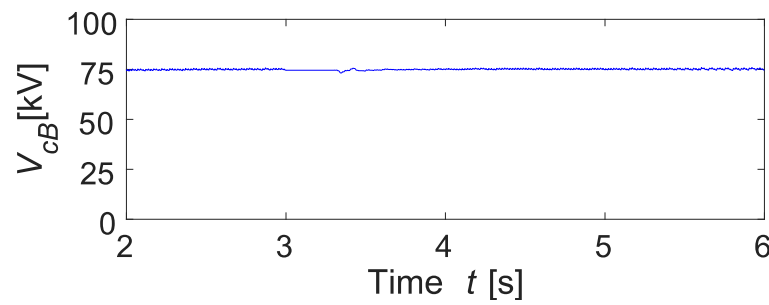


Figure 19. The voltage of the submodule capacitor outside the point of fault.

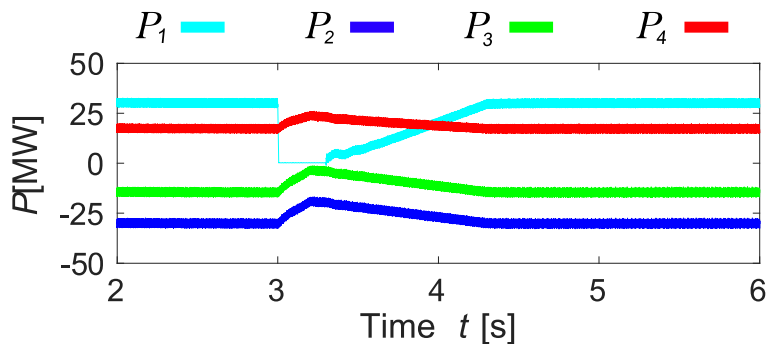


Figure 20. Active power.

5.4. Discussion

A comparison table is shown in Table 3. The ABB’s hybrid circuit breakers can eliminate HVDC system failures within 5 ms. However, hard switching in fault interruption was observed. The proposed hybrid circuit breaker can eliminate the fault of the HVDC system within 5 ms. ZCS was observed in fault interruption. In the fault simulation in the MTDC system, the circuit breaker showed sufficient fault rejection performance, and a stable system restart was observed.

Table 3. Comparison table.

	ABB's Breaker	Proposed Breaker
Switching	Hard Switching	ZCS (Soft Switching)
Interruption time	1.5 ms	1–1.1 ms

6. Conclusions

In this paper, a resonant hybrid DC circuit breaker for multi-terminal HVDC systems was proposed. The hard switching with conventional hybrid circuit breakers upon interruption has an adverse effect on the semiconductor switch. The resonant hybrid circuit breaker proposed in this paper provides soft-switching interruption and avoids the adverse effects of hard switching. The ABB's circuit breaker and the proposed circuit breaker were compared in a simulation. The ABB's circuit breaker has an interruption time of 1.5 ms and is suitable for the protection of HVDC systems. However, the current of 2 kA was rapidly interrupted, and hard switching was observed upon the fault current interruption. The proposed circuit breaker interrupts the current in 1 to 1.1 ms. The fault current is interrupted at the current zero point when the current is interrupted. Smooth reconnections of the system were confirmed to be about 1 s after fault clearing. Therefore, the proposed circuit breaker avoids the adverse effects of hard switching and can be applied to MTDC systems.

The proposed circuit breaker can be applied to the fault interruption of equipment handling high power in addition to current interruption of power lines. In the future, it is necessary to conduct simulations on transmission lines with distributed power sources, as well as experiments on actual equipment and simulations on high-power devices.

Author Contributions: Conceptualization, T.S.; methodology, R.M. and H.M.; software, H.T.; validation, R.M. and H.M.; formal analysis, R.M. and H.M.; investigation, R.M.; resources, A.N.; data curation, R.M.; writing—original draft preparation, R.M.; writing—review and editing, A.N.; visualization, A.M.H.; supervision, T.S.; project administration, T.S. All authors have read and agreed to the published version of the manuscript.

Funding: This research received no external funding.

Conflicts of Interest: The authors declare no conflict of interest.

Nomenclature

The following notations are used in this manuscript.

Abbreviations

AC	Alternating current
DC	Direct current
EMI	Electromagnetic interference
FB	Full bridge
HB	Half bridge
HVDC	High-voltage direct current
LCS	Load commutation switch
MOV	Metal oxide varistor
MTDC	Multi-terminal direct current
RBSOA	Reverse bias safety operation area
UFD	Ultrafast disconnecter
ZCS	Zero-current switching

Variables

C	Line capacitor during the fault [F]
C_{dc}	DC capacitor [F]
C_{re}	Resonant capacitor [F]
C_s	Snubber capacitor [F]
C_{SM}	Cell capacitor [F]
i_{Aa}, i_{Ab}, i_{Ac}	Current of upper arm [A]

i_{Ba}, i_{Bb}, i_{Bc}	Current of lower arm [A]
$I_{dc1} - I_{dc4}$	Transmission line current of each converter [A]
i_{ms}	Mechanical switch current of DC circuit breaker [A]
i_{ss}	Semiconductor switch current of DC circuit breaker [A]
i_{are}	MOV current of DC circuit breaker [A]
L	Line inductance during the fault [H]
l	Transmission distance [km]
L_{dc}	DC inductance [H]
L_{line}	Transmission line inductance [H]
n	The number of submodules
$P_1 - P_4$	Active power of each converter [MW]
R	Line resistance during the fault [Ω]
L_s	Suppression inductance [H]
R_{line}	Transmission line resistance [Ω]
v_{cAa1}, v_{cAa2}	The voltage of the upper-arm cell capacitor in phase a [V]
v_{cAb1}, v_{cAb2}	The voltage of the upper-arm cell capacitor in phase b [V]
v_{cAc1}, v_{cAc2}	The voltage of the upper-arm cell capacitor in phase c [V]
v_{cBa1}, v_{cBa2}	The voltage of the lower-arm cell capacitor in phase a [V]
v_{cBb1}, v_{cBb2}	The voltage of the lower-arm cell capacitor in phase b [V]
v_{cBc1}, v_{cBc2}	The voltage of the lower-arm cell capacitor in phase c [V]
$V_{dc1} - V_{dc4}$	DC link voltage [V]

References

- Liu, L.; Lotfy, M.; Matayoshi, H.; Senjyu, T.; Datta, M. Load Frequency Control for Renewable Energy. Sources for Isolated Power System. In Proceedings of the 5th International Conference on Electric Power and Energy Conversion Systems (EPECS) 2018, Kitakyushu, Japan, 23–25 April 2018; pp. 1–6. [\[CrossRef\]](#)
- Kinjo, R.; Matayoshi, H.; Ludin, G.; Howlader, A.; Urasaki, N.; Senjyu, T. Multi-Terminal High Voltage. Direct Current Transmission System with DC Resonant Semiconductor Breakers. *Int. J. Emerg. Electr. Power Syst.* **2018**. [\[CrossRef\]](#)
- Akila, A.; Helal, A.; Eldosouki, H. Protection of Active Distribution Systems with DGs. *Int. J. Emerg. Electr. Power Syst.* **2015**, *16*. [\[CrossRef\]](#)
- Park, K.H.; Lee, H.Y.; Asif, M.; Lee, B.W. Investigation of Arc Behavior in HVDC LC Resonance Circuit Breaker Using Flexible Pulsed DC-Source. In Proceedings of the 2018 Condition Monitoring and Diagnosis (CMD), Perth, Australia, 23–26 September 2018; pp. 1–5. [\[CrossRef\]](#)
- Nagoya, H.; Komami, S.; Ogimoto, K. A Method for Presuming Total Output Fluctuation of Highly Penetrated Photovoltaic Generation Considering Mutual Smoothing Effect. *IEEE Trans. Electron. Inf. Syst.* **2011**, *131*, 1688–1696. [\[CrossRef\]](#)
- Oozeki, T.; Takashima, T.; Otani, K.; Hishikawa, Y.; Koshimizu, G.; Uchida, Y.; Ogimoto, K. Statistical Analysis of the Smoothing Effect for Photovoltaic Systems in a Large Area. *IEEE Trans. Power Energy* **2010**, *130*, 491–500. [\[CrossRef\]](#)
- Yanxun, G.; Wang, G.; Zeng, D.; Li, H.; Hong, C. A Thyristor Full-Bridge-based DC Circuit Breaker. *IEEE Trans. Power Electron.* **2019**, *35*, 1111–1123. [\[CrossRef\]](#)
- Mobarrez, M.; Kashani, M.; Bhattacharya, S.; Adapa, R. Comparative study of DC circuit breakers using realtime simulations. In Proceedings of the 40th Annual Conference of the IEEE Industrial Electronics Society, Dallas, TX, USA, 29 October–1 November 2014; pp. 3736–3742. [\[CrossRef\]](#)
- Kimura, R.; Yokoyama, A.; Sano, K. DC Fault Clearing Characteristics of a Bulk Power VSC HVDC Transmission System using DC Circuit Breakers. *Electr. Eng. Jpn.* **2016**, *197*, 18–28. [\[CrossRef\]](#)
- Sano, K.; Takasaki, M. A Surgeless Solid-State DC Circuit Breaker for Voltage-Source-Converter-Based HVDC Systems. *IEEE Trans. Ind Appl.* **2014**, *50*, 2690–2699. [\[CrossRef\]](#)
- Gu, X.; He, S.; Xu, Y.; Yan, Y.; Hou, S.; Fu, M. Partial discharge detection on 320 kV VSC-HVDC XLPE cable with artificial defects under DC voltage. *IEEE Trans. Dielectr. Electr. Insul.* **2018**, 939–946. [\[CrossRef\]](#)
- Rodríguez, J.; Lai, J.S.; Peng, F. Multilevel inverters: A survey of topologies, controls, and applications. *IEEE Trans. Ind. Electron.* **2002**, *49*, 724–738. [\[CrossRef\]](#)

13. Meyer, C.; Kowal, M.; De Doncker, R. Circuit breaker concepts for future high-power DC-applications. In Proceedings of the Fourtieth IAS Annual Meeting. Conference Record of the 2005 Industry Applications Conference, Hong Kong, China, 2–6 October 2005; Volume 2, pp. 860–866. [CrossRef]
14. Nabae, A.; Takahashi, I.; Akagi, H. A neutral-point-clamped PWM inverter. *IEEE Trans. Ind. Appl.* **1981**, *7*, 518–523. [CrossRef]
15. Peng, F. A generalized multilevel inverter topology with self voltage balancing. *IEEE Trans. Ind. Appl.* **2001**, *37*, 611–618. [CrossRef]
16. Hui, L.; Poh, C.L.; Blaabjerg, F. Review of fault diagnosis and fault-tolerant control for modular multilevel converter of HVDC. In Proceedings of the IECON 2013—39th Annual Conference of the IEEE Industrial Electronics Society, Vienna, Austria, 10–13 November 2013; pp. 1242–1247. [CrossRef]
17. Norrga, S.; Li, X.; Ängquist, L. Converter topologies for HVDC grids. In Proceedings of the 2014 IEEE International Energy Conference (ENERGYCON), Cavtat, Croatia, 13–16 May 2013; pp. 1554–1561. [CrossRef]
18. Sheng, B. A Synthetic test circuit for current switching tests of HVDC circuit breakers. In Proceedings of the 2008 IEEE/PES Transmission and Distribution Conference and Exposition, Chicago, IL, USA, 21–24 April 2008; Volume 1, p. 1. [CrossRef]
19. Candelaria, J.; Park, J.D. VSC-HVDC system protection: A review of current methods. In Proceedings of the 2011 IEEE/PES Power Systems Conference and Exposition, Phoenix, AZ, USA, 20–23 March 2011. [CrossRef]
20. Franck, C. HVDC Circuit Breakers: A Review Identifying Future Research Needs. *IEEE Trans. Power Deliv.* **2011**, *26*, 998–1007. [CrossRef]
21. Ray, A.; Rajashekara, K.; Satish Naik, B.; Pramanick, S. Coupled Inductor Based Zero Current Switching Hybrid DC Circuit Breaker Topologies. *IEEE Trans. Ind. Appl.* **2019**. [CrossRef]
22. Qu, L.; Yu, Z.; Huang, Y.; Zeng, R. Research on effect of circuit parameters on breaking characteristics of mechanical DC circuit breaker. *Electr. Power Syst. Res.* **2019**, *179*. [CrossRef]
23. Muriuki, J.; Muriithi, C.; Ngoo, L.; Nyakoe, G. Review of HVDC Circuit Breakers Topologies. *IOSR J. Electr. Electron. Eng.* **2017**, *12*, 109–117. [CrossRef]
24. Callavik, M.; Blomberg, A.; Häfner, J.; Jacobson, B. The Hybrid HVDC Breaker an Innovation Breakthrough Enabling Reliable HVDC Grids. 2012. Available online: <https://docplayer.net/48922020-The-hybrid-hvdc-breaker-an-innovation-breakthrough-enabling-reliable-hvdc-grids.html> (accessed on 19 September 2020).
25. Li, C.; Liang, J.; Wang, S. Interlink hybrid DC circuit breaker. *IEEE Trans. Ind. Electron.* **2018**, *1*. [CrossRef]
26. Wang, K.; Lee, F.C.Y.; Hua, G.; Borojevic, D. A comparative study of switching losses of IGBTs under hard-switching, zero-voltage-switching and zero-current-switching. In Proceedings of the 1994 Power Electronics Specialist Conference—PESC'94, Taipei, Taiwan, 20–25 June 1994; Volume 2, pp. 1196–1204. [CrossRef]
27. Emami, Z.; Farzanefard, H.; Motahari, S.R. EMI evaluation in hard switching and soft switching PWM flyback converters. 46–51. In Proceedings of the 1st Power Electronic & Drive Systems & Technologies Conference (PEDSTC), Tehran, Iran, 17–18 February 2010. [CrossRef]
28. Wang, Y.; Yuan, Z.; Fu, J.; Li, Y.; Zhao, Y. A feasible coordination protection strategy for MMC-MTDC systems under DC faults. *Int. J. Electric. Power Energy Syst.* **2017**, *90*, 103–111. [CrossRef]
29. Zhang, S.; Zou, G.; Huang, Q.; Gao, H. A Fast DC Line Protection for MMC-MTDC Grids Based on PSVTWs. In Proceedings of the 2019 IEEE Power & Energy Society General Meeting (PESGM), Atlanta, GA, USA, 4–8 August 2019; pp. 1–5. [CrossRef]
30. Tom, S.; Thomas, J. HVDC Transmission Line Protection Based on Transient Power. *Proc. Technol.* **2016**, *25*, 660–668. [CrossRef]

